ROYAL SOCIETY OPEN SCIENCE

royalsocietypublishing.org/journal/rsos

Research

Cite this article: Ahmed F, Awada C, Ansari SA, Aljaafari A, Alshoaibi A. 2019 Photocatalytic inactivation of *Escherischia coli* under UV light irradiation using large surface area anatase TiO_2 quantum dots. *R. Soc. open sci.* **6**: 191444. http://dx.doi.org/10.1098/rsos.191444

Received: 24 August 2019
Accepted: 16 September 2019

Subject Category:
Chemistry

Subject Areas:
nanotechnology/materials science/nanotechnology

Keywords:
TiO_2, quantum dots, microwave–hydrothermal, X-ray diffraction, photocatalysis

Authors for correspondence:
Faheem Ahmed
e-mail: fahmed@kfu.edu.sa
Chawki Awada
e-mail: cawada@kfu.edu.sa

This article has been edited by the Royal Society of Chemistry, including the commissioning, peer review process and editorial aspects up to the point of acceptance.

ROYAL SOCIETY OF CHEMISTRY

THE ROYAL SOCIETY PUBLISHING

Photocatalytic inactivation of *Escherischia coli* under UV light irradiation using large surface area anatase TiO_2 quantum dots

Faheem Ahmed, Chawki Awada, Sajid Ali Ansari, Abdullah Aljaafari and Adil Alshoaibi

Physics Department, College of Science, King Faisal University, Hofuf, Al-Ahsa 31982, Saudi Arabia

FA, 0000-0002-5436-1966

In this study, high specific surface areas (SSAs) of anatase titanium dioxide (TiO_2) quantum dots (QDs) were successfully synthesized through a novel one-step microwave–hydrothermal method in rapid synthesis time (20 min) without further heat treatment. XRD analysis and HR-TEM images showed that the as-prepared TiO_2 QDs of approximately 2 nm size have high crystallinity with anatase phase. Optical properties showed that the energy band gap (E_g) of as-prepared TiO_2 QDs was 3.60 eV, which is higher than the standard TiO_2 band gap, which might be due to the quantum size effect. Raman studies showed shifting and broadening of the peaks of TiO_2 QDs due to the reduction of the crystallite size. The obtained Brunauer–Emmett–Teller specific surface area (381 $m^2\ g^{-1}$) of TiO_2 QDs is greater than the surface area (181 $m^2\ g^{-1}$) of commercial TiO_2 nanoparticles. The photocatalytic activities of TiO_2 QDs were conducted by the inactivation of *Escherischia coli* under ultraviolet light irradiation and compared with commercially available anatase TiO_2 nanoparticles. The photocatalytic inactivation ability of *E. coli* was estimated to be 91% at 60 µg ml^{-1} for TiO_2 QDs, which is superior to the commercial TiO_2 nanoparticles. Hence, the present study provides new insight into the rapid synthesis of TiO_2 QDs without any annealing treatment to increase the absorbance of ultraviolet light for superior photocatalytic inactivation ability of *E. coli*.

1. Introduction

Titanium dioxide (TiO_2) is a significant nanomaterial which has attracted a considerable attention because of its distinctive

optoelectronic and photocatalytic properties. TiO_2 has catalytic, dielectric and optical properties, which leads to diverse industrial applications such as solar cell, pigments, fillers, catalyst supports and photo-catalysts [1–5]. Specifically, the TiO_2 nanoparticles-based photocatalysis technique is an important and promising method for the complete removal of organic compounds [6,7] and microorganisms [8,9]. In general, the organic compounds can be oxidized to carbon dioxide (CO_2), water and simple mineral acids at ambient temperature using TiO_2 nanoparticles under the illumination of ultraviolet source [10,11]. Recently, the development of TiO_2 and TiO_2–Pt catalyst efficiently interacts with the microbial cells under UV light source, showing the microbial cells were completely removed [12]. Moreover, various bacteria, cancerous cells, viruses, algae and fungi were successfully deactivated under the irradiation of UV source using TiO_2 nanoparticles [13–17]. Furthermore, Sunada *et al.* [18] reported that the TiO_2 nanoparticles are not only killed by the bacteria through photocatalytic process, but also they are used for the decomposition of toxic ingredient of bacteria. If the UV light illuminated for a reasonable time, the bacteria are completely mineralized and converted into CO_2, H_2O and other mineral substances [19,20]. On the other hand, the degradation efficiency of TiO_2 nanoparticles depends on their morphology, preparation methods and specially size of the particles. The small lateral sized TiO_2 nanoparticles exhibit higher specific surface areas (SSAs) [21]. In addition, when the size of TiO_2 decreased to below 10 nm, its energy band gap of TiO_2 increased due to its quantum size effect [22,23].

TiO_2 nanoparticles were prepared by many synthetic routes not limited to but including sol–gel method [24], hydrothermal process [25], template routes [26] and reverse micelles [27]. The sol–gel synthesis process is employed for the controlled synthesis of TiO_2 nanoparticles; however, the synthesis of smaller TiO_2 nanoparticles with homogeneous size distribution is still challenging. In general, TiO_2 nanoparticles prepared by a sol–gel method are amorphous in nature; therefore, a calcination process is required to achieve the crystallinity. Another factor that plays a key role in increasing the photocatalytic activity is the larger SSA of TiO_2. Although calcination process could be improved by the crystallinity of TiO_2 nanomaterials, it might induce the aggregation of small nanoparticles that leads to a decrease of the SSA. Based on the above concern, we need to synthesize agglomeration-free photocatalytic active TiO_2 nanoparticles without any further heat treatment.

Recently, Sofia *et al.* [28] used a novel sol–gel reflux condensation route to produce TiO_2 QDs. In their work, the process involved using titanium tetra-isopropoxide as the precursor that was hydrolysed and then subjected to reflux condensation for 24 h. Spherical QD morphology with an average crystallite size of 5–7 nm was obtained by subsequent drying and annealing (450°C for 1 h) treatments. In another report, Xu *et al.* [29] prepared TiO_2 quantum dots (QDs) by using an autoclave method, and the mixed solution was heated at 150°C for 24 h in autoclave. They reported that the final product was in the form of mixed structures of monodispersed QDs (3–6 nm) and islands (15–30 nm). Lalitha *et al.* [30] synthesized TiO_2 QDs by the sol–gel method. In their work, calcination at 350°C for 30 min was required to obtain TiO_2 QDs of 4.8 nm size. Deng *et al.* [31] synthesized anatase TiO_2 QDs with surface hydroxyl groups and particle size below 3 nm via a new synthetic route (sol–gel). They have reported that the reaction was completed in a Teflon-lined autoclave, and kept in an oven at 90°C for 1 day.

These reports showed that the preparation methods used for TiO_2 QDs are time- and energy-consuming and do not fulfil the economic and industrial requirements of TiO_2 QDs-based photo-catalysts. Thus, a simple and fast route, for the synthesis of TiO_2 QDs under ambient conditions without any annealing treatment, is still required. Compared with the above-mentioned techniques, microwave–hydrothermal method is much simpler and cheaper due to its unique features such as short reaction time, rapid and homogeneous volumetric heating, enhanced reaction selectivity, energy saving, environment-friendliness and high reaction rate [32].

In this work, we report the synthesis of the agglomeration-free anatase TiO_2 quantum dot, for the first time, by using $TiCl_3$ and NaOH by microwave–hydrothermal method toward the photocatalytic deactivation of *Escherischia coli* under UV light source. The microwave-assisted hydrothermal process is adopted to synthesize with controlled size and shape of TiO_2 QDs. Most importantly, there is no requirement of further calcination steps to obtain final product as was required in earlier reports [28–31]. The resulting QDs show remarkably high photocatalytic inactivation of *E. coli* as compared with commercially available TiO_2 nanoparticles.

2. Experimental details

Analytical grade precursors and reagents were used in the present experiments. The synthesis was performed in a microwave–hydrothermal system (CEM-MARS 5). For the synthesis, to prepare aqueous solution, $TiCl_3$

(Sigma Aldrich) and NaOH (99.99%; Sigma Aldrich) in 1 : 10 molar ratio were dissolved in 50 ml deionized water (Milli-Q Gradient A-10 system (Millipore)). The solution was stirred for 20 min at room temperature and transferred into a 100 ml Teflon-lined digestion vessel at 160°C for 20 min with a pressure in the range of 150 psi and 500 W power in a microwave–hydrothermal. After completing the reaction, the solution was cooled down to room temperature. The precipitate was collected and washed several times with water and ethanol. The final samples were dried in an oven at 80°C for 24 h. For the comparison purpose, commercial TiO_2 nanoparticles (Anatase, nanopowder, 99.7%; Sigma Aldrich) were used.

X-ray diffraction (XRD) analysis of the samples was carried out using a Phillips X'pert (MPD-3040) X-ray diffractometer with Cu Kα radiation ($\lambda = 1.5406$ Å) operated at a current of 30 mA and a voltage of 40 kV. The morphological studies of QDs were explored through high-resolution transmission electron microscopy (HR-TEM; JEOL/JEM-2100F) operated at 200 kV and a field emission scanning electron microscope (FESEM; MIRA II LMH). UV–Vis spectrophotometer (Agilent-8453) was used to obtain the optical behaviour of the samples ranging from 200 to 800 nm. The optical band gap of the QDs was determined from the UV–Vis diffuse reflectance spectra recorded at room temperature. Raman spectrometer (NRS-3100, $\lambda = 532$ nm) was used to study the structural properties of TiO_2 QDs. The SSA of the samples was estimated using Brunauer–Emmett–Teller (BET; Autosorb-1, Quantachrome) analysis.

In photocatalytic experiments, 20, 40 and 60 µg ml^{-1} of aqueous TiO_2 solution was prepared through the normal saline water under dark condition. Afterwards, 10 ml of TiO_2 solution and 10% fresh standard inoculums of *E. coli* ($\approx 10^8$ cfu ml^{-1}) were added into 80 ml sterilized normal saline. For the standardization of the overnight grown culture, where standard inoculum is prepared by diluting and making a 10% inoculum in fresh broth. This fresh 10% inoculum is equivalent to approximately 10^8 cfu ml^{-1}. Before the light exposure, the suspension was stirred with a magnetic stirrer for 30 min in the dark condition. During the dark experiment and irradiation, the beaker was wrapped with an aluminium foil to shield it from the ambient light and to increase reflection. The complete suspension was stirred through the magnetic stirrer, while UV light (Spectronics ENF-240C, ($\lambda = 365$ nm) 4 W tubes) at 15 cm distance from the surface of the medium was illuminated and the suspension was collected every 30 min interval for 4 h. The viable concentration of *E. coli* was estimated with dispersion plate method on nutrient agar. For control, experiment was conducted without the addition of TiO_2 into *E. coli* suspension under UV light irradiation. The collected plates were incubated at 37°C for 24 h and the colony counter was used for counting the colonies. For a comparative study, similar concentrations of 20, 40 and 60 µg ml^{-1} of commercial TiO_2 nanoparticles solution were used.

3. Results and discussion

Figure 1 depicts the XRD patterns of the as-prepared TiO_2 QDs and the commercial TiO_2 nanoparticles. All the diffractions peaks in TiO_2 QDs and commercial nanoparticles are well matched and indexed to anatase phase, and are in good agreement with standard JCPDS card no. 89-4921. From this pattern, the as-synthesized TiO_2 QDs exhibit well crystalline peaks with pure anatase, indicating the complete crystallization of the stable anatase phase without any further heat treatment. Mainly, the localized high temperatures through microwaves caused the rapid crystallization of TiO_2 QDs [33]. The major diffraction peaks of TiO_2 QDs indicate at the same peak position (2θ) as commercial TiO_2 nanoparticles. Moreover, the major peak of TiO_2 QDs shows broader and the relative peak intensity decreases, which indicates very smaller crystallite size. The average crystallite size (D) of TiO_2 QDs and commercial nanoparticles estimated using Debye–Scherrer formula [34] using most intense (101) plane diffraction peaks were found to be approximately 2 nm and approximately 20 nm, respectively.

To identify the morphology and dimension of the TiO_2 QDs and commercial TiO_2 nanoparticles, FESEM and TEM were used. FESEM images (low magnification) of the TiO_2 QDs showed nanoparticles ranging from 2 to 5 nm (figure 2*b*), which can be seen in the high-magnification images as shown in the inset of figure 2*b*. On the other hand, commercial nanoparticles of TiO_2 are larger ranging 20–30 nm (figure 2*a*).

Moreover, TEM and HRTEM studies were performed to get the information about morphologies and the structural features of TiO_2 QDs. Figure 3 displays the TEM image (low magnification) of the TiO_2 QDs of approximately 2 nm size (upper inset of figure 3) which is well matched with the XRD analysis and uniformly distributed (lower inset of figure 3). The HRTEM image (figure 4) displays clear lattice fringes of as-prepared QDs, and it was completely crystalline and entirely consists of an anatase phase. The lattice spacing d is 0.34 nm corresponding to the (101) crystallographic planes of anatase TiO_2.

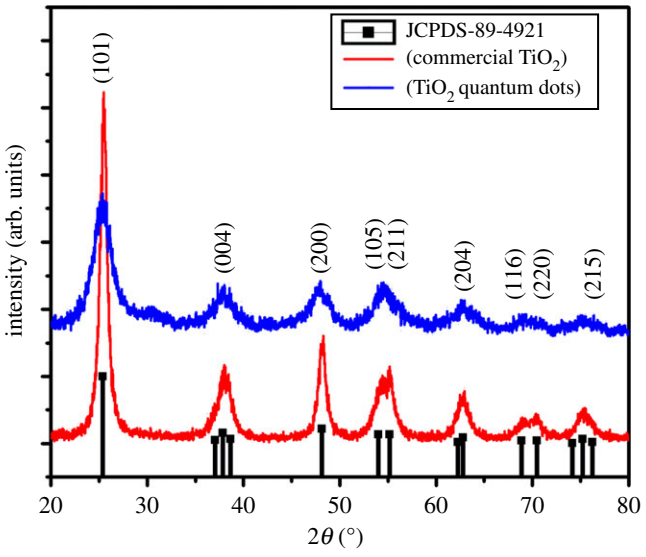

Figure 1. XRD patterns of as-synthesized TiO_2 QDs, commercial TiO_2 nanoparticles and standard JCPDS 89-4921 of TiO_2.

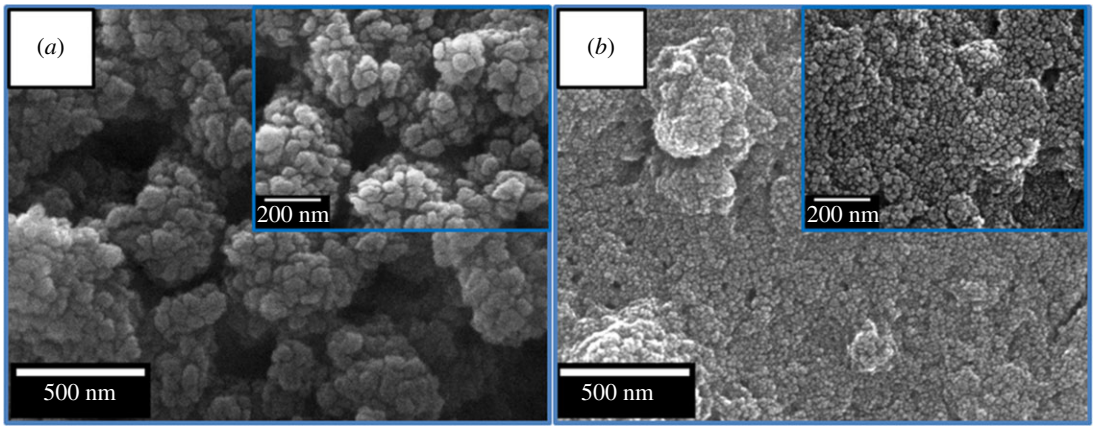

Figure 2. Low magnification FESEM images of (*a*) commercial TiO_2 nanoparticles, (*b*) TiO_2 QDs. Insets of (*a*) and (*b*) show high-magnification FESEM images.

To study the quantum confinement effect of as-prepared TiO_2 QDs on the band gap, UV–Vis spectroscopy was employed. Figure 5*a* shows the UV–Vis diffuse reflectance spectra of TiO_2 QDs and commercial TiO_2 nanoparticles. The band gap energies of the TiO_2 QDs and commercial TiO_2 nanoparticles were evaluated using Kubelka–Munk function [35,36]. The plot of $(F(R)hv)^2$ versus photon energy (hv) for TiO_2 QDs and commercial TiO_2 nanoparticles is shown in figure 5*b*. The energy band gap of TiO_2 QDs was found to be 3.60 eV which is larger than the value of commercial TiO_2 nanoparticles as well as the reported value for anatase (3.2 eV) [37]. This increase in E_g might be due to the quantum size effect [38].

Raman spectrum carried out at room temperature further supported the formation of a tetragonal anatase structure of TiO_2 QDs confirmed in the XRD. An earlier report [39] showed that for anatase TiO_2, six Raman active modes, i.e. A_1g, two B_1g and three Eg, were obtained, and could be detected at 144 cm^{-1} (E_g), 197 cm^{-1} (E_g), 399 cm^{-1} (B_1g), 513 cm^{-1} (A_1g), 519 cm^{-1} (B_1g) and 639 cm^{-1} (E_g). Figure 6 illustrates the Raman spectra of both samples, which indicate the presence of anatase phases TiO_2 for both the QDs and commercial nanoparticles. Moreover, the peak corresponding to the B_1g mode, A_1g and Eg modes of TiO_2 QDs shows significant broadening and a small shift toward the higher frequencies than that of the commercial TiO_2 (figure 6). It is well known that this shift is attributed to the phonon confinement size effect [40]. In the present work, TiO_2 QDs are of approximately 2 nm size; thus, the shift of Raman peaks is due to the quantum size effect.

The SSA of TiO_2 plays a key role in photocatalysis [41]. Thus, the primary objective was to prepare larger SSA TiO_2 QDs. Figures 7*a* and 8*a* show the nitrogen adsorption–desorption isotherms, and the

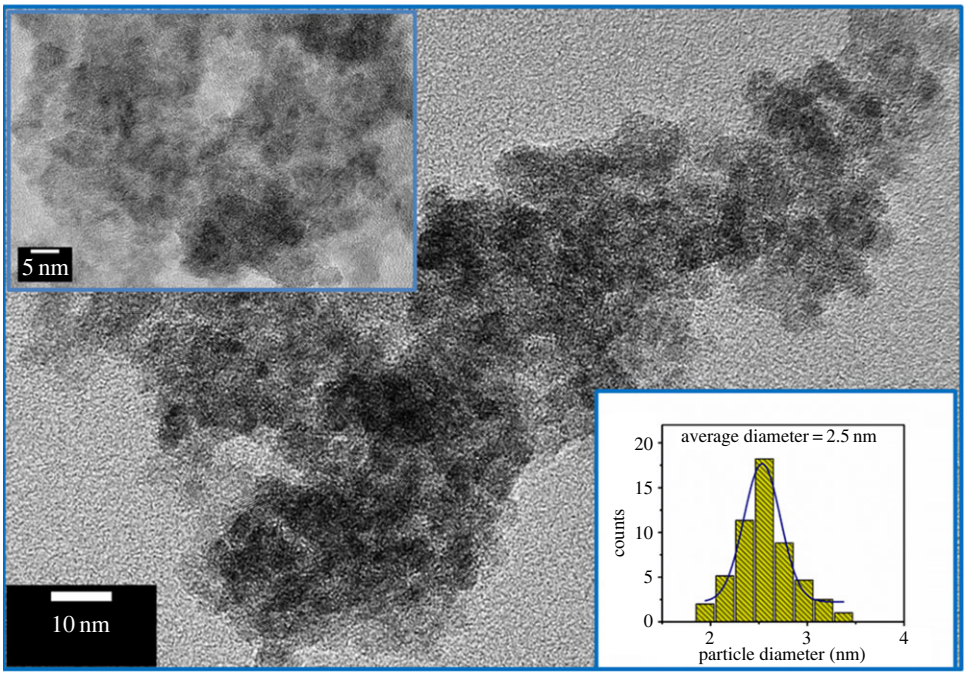

Figure 3. TEM image of TiO_2 QDs (low magnification), the upper inset shows high-magnification TEM images and the lower inset shows corresponding particle size distribution plot.

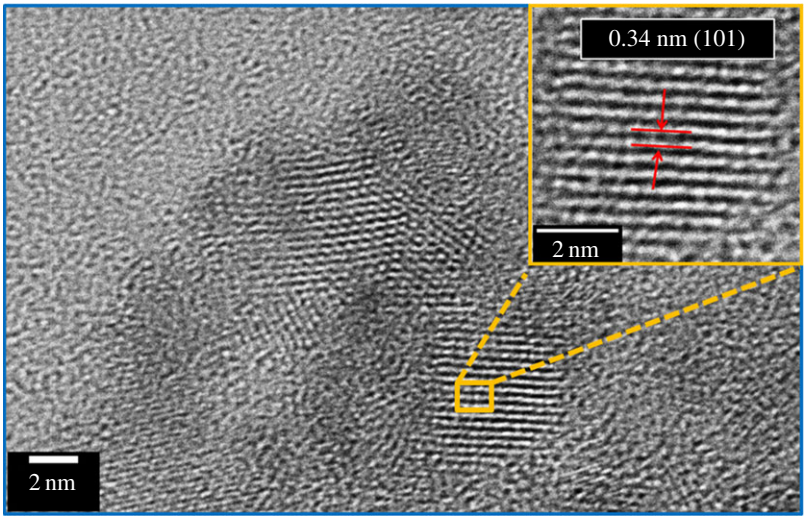

Figure 4. HRTEM image of TiO_2 QDs, inset shows high-magnification image of the zoomed area.

SSA plot of the as-synthesized TiO_2 QDs and commercial TiO_2 nanoparticles are shown in figures 7*b* and 8*b*, respectively. The isotherm shows that the nitrogen adsorption volume gradually increases with the relative pressure and then decreases with the decrease of relative pressure (figure 7*a*). The SSA of the TiO_2 QDs was calculated to be approximately 381 $m^2\ g^{-1}$ (figure 7*b*) higher than that of commercial TiO_2 particles of approximately 181 $m^2\ g^{-1}$ (figure 8*b*). Also, the TiO_2 QDs synthesized by this method showed higher SSA than already reported TiO_2 nanoparticles. Yan *et al*. [42] reported preparation of TiO_2 nanoparticles with diameter ranging 4–12 nm having an SSA of approximately 64 $m^2\ g^{-1}$, on the other hand, Suttiponparnit *et al*. [43] showed an SSA of 254 $m^2\ g^{-1}$ of TiO_2 nanoparticles. In addition, Lee *et al.* [44] reported TiO_2 nanoparticles produced from the sludge of $TiCl_4$ flocculation of wastewater and seawater with average crystallite sizes of 6, 15 and 40 nm with the surface area of 76, 103 and 168 $m^2\ g^{-1}$, respectively from artificial wastewater (AW), biologically treated sewage effluent (BTSE) and seawater (SW), respectively. By comparing our results with these reports, the synthesized QDs in this study have a smaller particle size of approximately 2 nm and very large SSA of 381 $m^2\ g^{-1}$, thus the presented

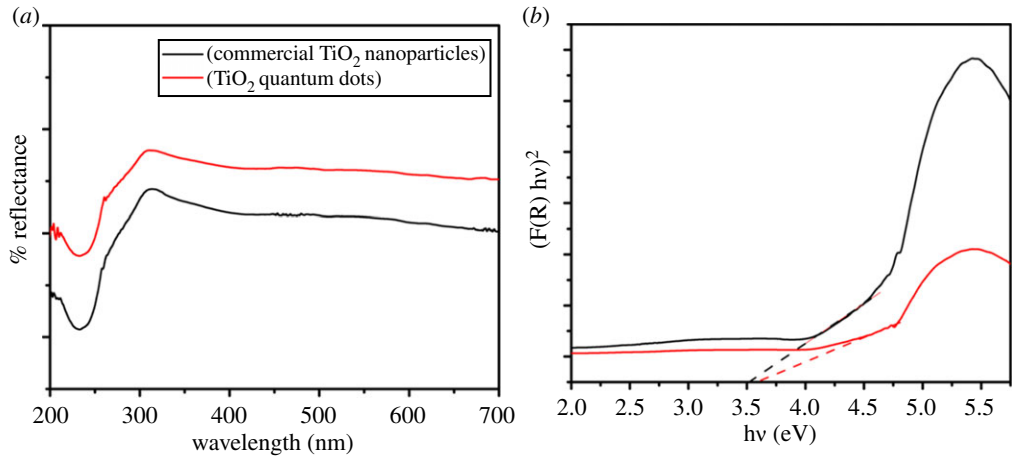

Figure 5. (*a*) UV–Vis diffuse reflectance spectra, and (*b*) Kubelka–Munk plots for TiO_2 QDs and commercial TiO_2 nanoparticles.

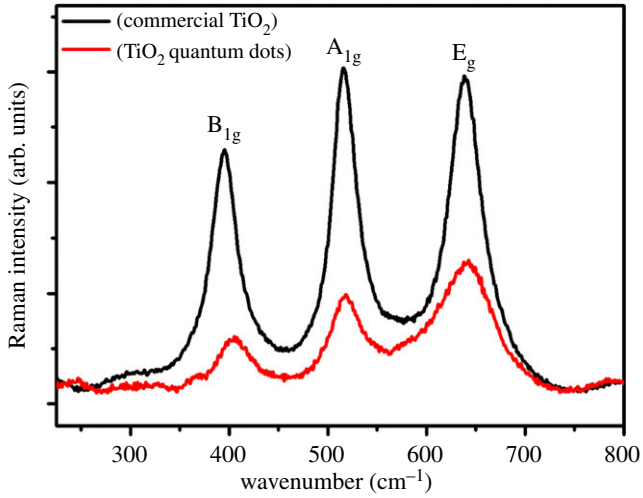

Figure 6. Raman spectra of TiO_2 QDs and commercial TiO_2 nanoparticles.

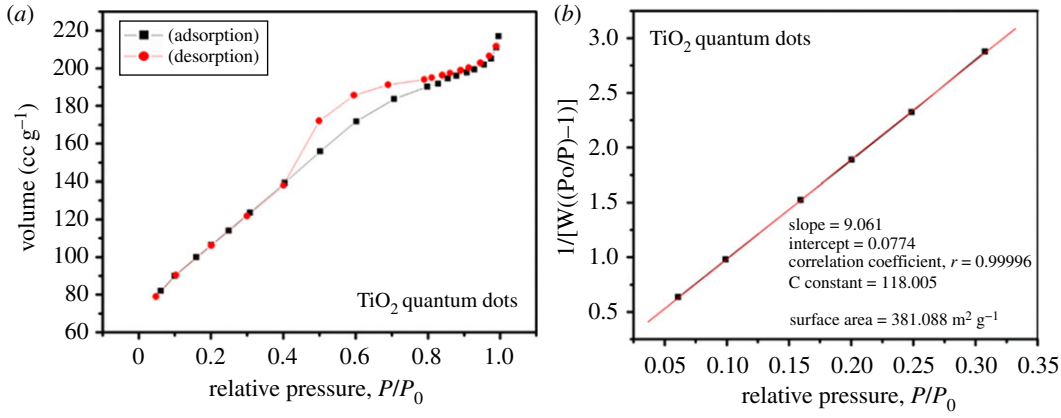

Figure 7. (*a*) Nitrogen adsorption–desorption isotherm of as-synthesized TiO_2 QDs, (*b*) corresponding BET surface area plot.

method is more efficient to produce QDs with large SSA. The higher SSA of TiO_2 could enhance the surface reactivity [45].

Furthermore, the photocatalytic deactivation of *E. coli* was conducted by TiO_2 QDs and commercial TiO_2 nanoparticles powder concentration ranging from 20 to 60 µg ml^{-1} under UV light irradiation, as shown in figure 9. The nanomaterial will show stronger antibacterial activity if the change occurs in

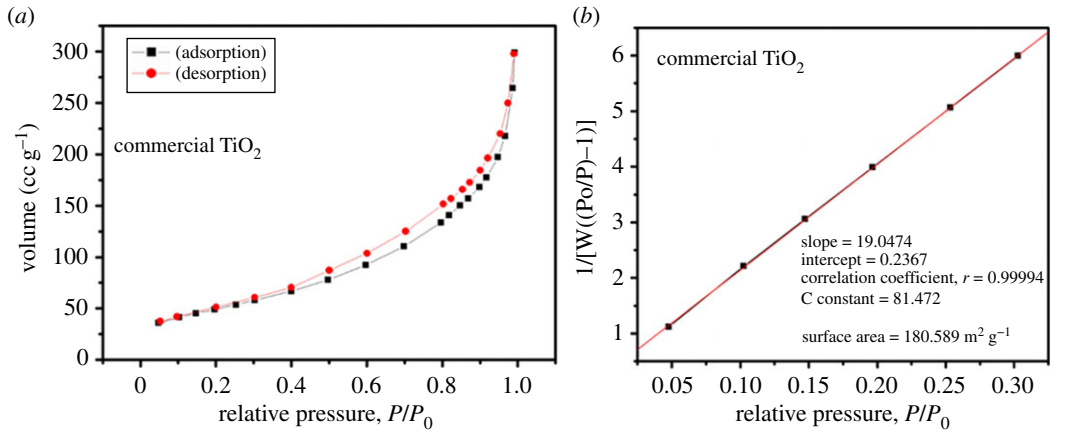

Figure 8. (*a*) Nitrogen adsorption–desorption isotherm of commercial TiO_2 nanoparticles, (*b*) corresponding BET surface area plot.

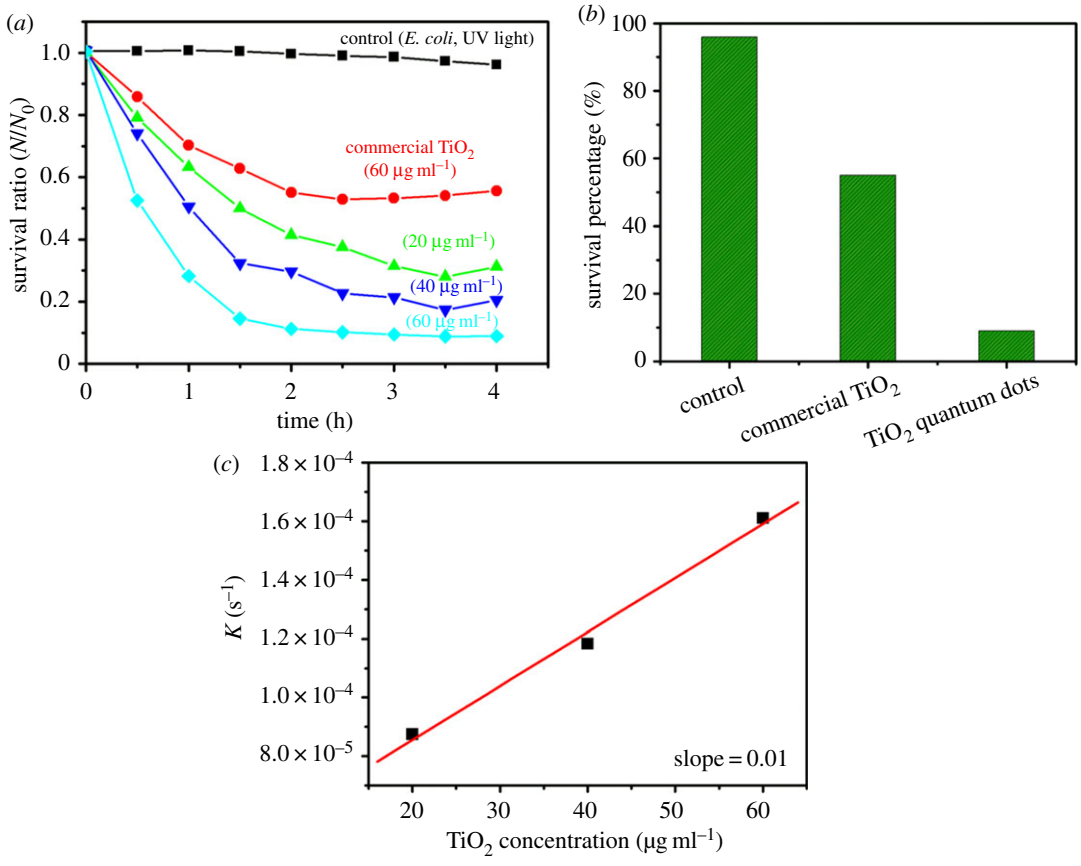

Figure 9. (*a*) Plot of change in the survival ratio of *E. coli*, (*b*) survival percentage of *E. coli*, (*c*) the relation between death rate constant and TiO_2 QDs concentration towards *E. coli*.

the survival ratio (N/N_0; N = number of cells at time t, N_0 = number of cell at time $t = 0$) with the specified time. It is clear from figure 9*a* that with the increase of UV irradiation time, the survival ratio decreased, which is illustrating the inactivation of *E. coli*. At a specified time, with the increase in powder concentration, the values became smaller, which showed that the higher the powder concentration, the higher the antibacterial activity. In particular, the survival ratio of TiO_2 QDs decreased more steeply in short time as compared with commercial TiO_2 nanoparticles. Figure 9*b* shows the survival percentage of *E. coli* for control, commercial TiO_2 nanoparticles and TiO_2 QDs. It was observed that the highest inactivation of 91% of *E. coli* was achieved in the presence of 60 µg ml^{-1} of TiO_2 QDs, while only 45 and 3% of *E. coli* were inactivated in the presence of commercial TiO_2 nanoparticles and control, respectively. It is clear that the TiO_2 QDs show higher photocatalytic inactivation of *E. coli*

than the commercial nanoparticles. By converting the survival ratio of vertical axis into logarithmic value as depicted in figure 9*a*, a linear decrease for time resulted to the ratio. Thus, death rate constant, k can be determined by first-order kinetics [46];

$$\frac{dN}{dt} = -KN, \tag{3.1}$$

where N corresponds to survival ratio (N/N_0) and t is the time. Figure 9*c* shows the relationship between K value and TiO_2 QDs concentration. The slope value in death rate constant plot of *E. coli* was found to be approximately 0.01. In comparison with photocatalysis-based antibacterial activity of TiO_2 QDs and commercial TiO_2 nanoparticles towards *E. coli*, it was found that the antibacterial activity of TiO_2 QDs were much stronger than the commercial TiO_2 nanoparticles.

Different activity of the prepared samples is associated with their SSA and the size of the particles. It has been reported that ultra-small particles (i.e. quantum-sized particles) showed better photochemical characteristics than Degussa P25 [47], and have the characteristics between molecular and bulk semiconductor. Thus, there is improvement in the surface-limited reactions due to high surface area-to-volume ratios [45], since TiO_2 QDs are purely anatase phase and have extremely large SSA as compared with commercial nanoparticles, which provides better reactivity with the microorganisms and resulted in higher photocatalytic inactivation.

Sunada *et al*. [48] reported that the photocatalytic mechanism using TiO_2 on *E. coli* is a three-stage process where the decomposition of the dead cell occurred. Fujishima *et al*. [49] showed that *E. coli* will be totally mineralized with the illumination time.

In a photocatalytic process, the light with a wavelength greater than or equal to the band gap (E_g) of the semiconductor irradiates onto a semiconductor such as TiO_2. When the QDs absorb the light, the electrons in the valance band excited to the conduction band, resulting in the generation of photoexcited electron–hole pairs. These photoexcited electron–holes might diffuse to the surface of the semiconductor resulted in the interfacial electron transfer. The oxidation reactions in the solution are caused by holes which resulted in the mineralization of organic substances [50]. In the photocatalytic process, $OH^{\bullet}$ radicals formed which are governed by OH groups and or physisorbed H_2O. The production of highly reactive hydroxyl radicals ($OH^{\bullet}$) occurred due to the reaction of holes with water, and caused the oxidation of organic materials and biomolecules [51]. To achieve a high efficiency by the adsorption of higher OH groups on the surface of QDs, the large SSA of the TiO_2 QDs is a key factor. In another factor the wider band gap of TiO_2 QDs prevents the recombination effects of charge carriers, resulting in higher photocatalytic activity against *E. coli*. Moreover, when the crystallite size of the particle decreases to below or approximately 10 nm, the charge carriers acted quantum mechanically [45]. Due to the confinement, the band gap increased with the decrease of particle size. Thus, with the increase in band gap, the potential of oxidation of the photon-generated holes and the reducing potential of the electrons might increase. Consequently, TiO_2 QDs exhibit excellent photocatalytic properties, and this property was used for the inactivation of *E. coli*.

4. Conclusion

In summary, rapid and cost-effective one-pot microwave–hydrothermal route was used to prepare anatase TiO_2 QDs within 20 min without any additional heat treatment, and the photocatalytic inactivation of *E. coli* was investigated. XRD, Raman and HRTEM investigations confirmed the tetragonal anatase structure with well crystalline and single-phase nature. TEM results revealed TiO_2 QDs with the size of approximately 2 nm. The BET surface area analysis showed that the anatase TiO_2 QDs exhibited a much higher SSA (381 $m^2\,g^{-1}$) than commercial nanoparticles (181 $m^2\,g^{-1}$) as well as earlier reported TiO_2. The band gap energy for QDs was found to be 3.60 eV higher than that of the commercial nanoparticles. As-synthesized TiO_2 QDs exhibit higher photocatalytic inactivation of *E. coli* than commercially available nanoparticles under UV light irradiation. TiO_2 concentration of 60 µg ml^{-1} is sufficient to inactivate about 91% of *E. coli*. The higher photocatalytic inactivation properties of the TiO_2 QDs are believed to be due to smaller particle size and higher band gap resulted in the higher SSA and prevent electron–hole recombination rate compared with the commercial nanoparticles. These QDs effectively inactivate *E. coli* by photocatalysis and offer an improved charge separation and promote the photoactivity significantly. This work suggests that to obtain excellent photocatalytic properties, tuning of particle size might be a key parameter for promising future biomedical applications.

Data accessibility. Data available from the Dryad Digital Repository: https://dx.doi.org/10.5061/dryad.9pc7mj1 [52].
Authors' contributions. F.A. designed the study and prepared all the samples for analysis. F.A., S.A.A. and C.A. collected and analysed the data. F.A., A.A., and A.A.S. contributed in interpreting the results and writing the manuscript. All authors read the manuscript and gave final approval for publication.
Competing interests. The authors declare no competing interest.
Funding. This work is funded by Deanship of Scientific Research at King Faisal University through NASHER track (grant no. 186101).
Acknowledgements. The authors would like to thank the Deanship of Scientific Research at King Faisal University for supporting this research through NASHER track (grant no. 186101).

References

1. Barbé CJ, Arendse F, Comte P, Jirousek M, Grätzel M. 1997 Nanocrystalline titanium oxide electrodes for photovoltaic applications. *J. Am. Ceram. Soc.* **80**, 3157–3171. (doi:10.1111/j.1151-2916.1997.tb03245.x)
2. Monticone R, Tufeu AV, Kanaev E, Scolan C, Sanchez C. 2000 Quantum size effect in TiO_2 nanoparticles: does it exist? *Appl. Surf. Sci.* **162–163**, 565–570. (doi:10.1016/S0169-4332(00)00251-8)
3. Boujday S, Wunsch F, Portes P, Bocquet J-F, Justin CC. 2004 Photocatalytic and electronic properties of TiO_2 powders elaborated by sol–gel route and supercritical drying. *Solar Energy Mater. Solar Cells* **83**, 421–433. (doi:10.1016/j.solmat.2004.02.035)
4. Carp O, Huisman CL, Reller A. 2004 Photoinduced reactivity of titanium dioxide. *Prog. Solid State Chem.* **32**, 33–177. (doi:10.1016/j.progsolidstchem.2004.08.001)
5. Ruiz AM, Sakai G, Cornet A, Shimanoe K, Morante JR, Yamazoe N. 2004 Microstructure control of thermally stable TiO_2 obtained by hydrothermal process for gas sensors. *Sens. Actuators B: Chem.* **103**, 312–317. (doi:10.1016/j.snb.2004.04.061)
6. Wang XH, Li JG, Kamiyama H, Moriyoshi Y, Ishigaki T. 2006 Wavelength-sensitive photocatalytic degradation of methyl orange in aqueous suspension over iron(III)-doped TiO_2 nanopowders under UV and visible light irradiation. *J. Phys. Chem. B* **110**, 6804–6809. (doi:10.1021/jp060082z)
7. Padmanabhan SC, Pillai SC, Colreavy J, Balakrishnan S, McCormack DE, Perova TS, Gun'ko Y, Hinder SJ, Kelly JM. 2007 A simple sol—gel processing for the development of high-temperature stable photoactive anatase titania. *Chem. Mater.* **19**, 4474–4481. (doi:10.1021/cm070980n)
8. Fu G, Vary PS, Lin CT. 2005 Anatase TiO_2 nanocomposites for antimicrobial coatings. *J. Phys. Chem. B* **109**, 8889–8898. (doi:10.1021/jp0502196)
9. Seo JW, Chung H, Kim MY, Lee J, Chio IH, Cheon JW. 2007 Development of water-soluble single-crystalline TiO_2 nanoparticles for photocatalytic cancer-cell treatment. *Small* **3**, 850–853. (doi:10.1002/smll.200600488)
10. Zuo GM, Cheng ZX, Chen H, Li GW, Miao T. 2006 Study on photocatalytic degradation of several volatile organic compounds. *J. Hazard. Mater.* **128**, 158–163. (doi:10.1016/j.jhazmat.2005.07.056)
11. Tsoukleris DS, Maggos T, Vassilakos C, Falaras P. 2007 Photocatalytic degradation of volatile organics on TiO_2 embedded glass spherules. *Catal. Today* **129**, 96–101. (doi:10.1016/j.cattod.2007.06.047)
12. Matsunaga T, Tomoda R, Nakajima T, Wake H. 1985 Photoelectrochemical sterilization of microbial cells by semiconductor powders. *FEMS Microbiol. Lett.* **29**, 211–214. (doi:10.1111/j.1574-6968.1985.tb00864.x)
13. Ji LY, Yuan MM, Xiaohu W, Xiaohua W. 2008 Inactivated properties of activated carbon-supported TiO_2 nanoparticles for bacteria and kinetic study. *J. Environ. Sci.* **20**, 1527–1533. (doi:10.1016/S1001-0742(08)62561-9)
14. Kuhn KP, Chaberny IF, Massholder K, Sticker M, Benz VW, Sonntag HG, Erdinger L. 2003 Disinfection of surfaces by photocatalytic oxidation with titanium dioxide and UVA light. *Chemosphere* **53**, 71–77. (doi:10.1016/S0045-6535(03)00362-X)
15. Thevenot P, Cho J, Wavhal D, Timmons RB, Tang L. 2008 Surface chemistry influences cancer killing effect of TiO_2 nanoparticles. *Nanomedicine* **4**, 226–236. (doi:10.1016/j.nano.2008.04.001)
16. Zan L, Fa WJ, Peng TY, Gong ZK. 2007 Photocatalysis effect of nanometer TiO_2 and TiO_2-coated ceramic plate on hepatitis B virus. *J. Photochem. Photobiol. B: Biol.* **86**, 165–169. (doi:10.1016/j.jphotobiol.2006.09.002)
17. Seven O, Dindar B, Aydemir S, Metin D, Ozinel MA, Idi S. 2004 Solar photocatalytic disinfection of a group of bacteria and fungi aqueous suspensions with TiO_2, ZnO and Sahara desert dust. *J. Photochem. Photobiol. A: Chem.* **165**, 103–107. (doi:10.1016/j.jphotochem.2004.03.005)
18. Sunada K, Kikuchi Y, Hashimoto K, Fujishima A. 1998 Bactericidal and detoxification effects of TiO_2 thin film photocatalysts. *Environ. Sci. Technol.* **32**, 726–728. (doi:10.1021/es970860o)
19. Jacoby WA, Maness BC, Wolfrum EJ, Blake DM, Fennell JA. 1998 Mineralization of bacterial cell mass on a photocatalytic surface in air. *Environ. Sci. Technol.* **32**, 2650–2653. (doi:10.1021/es980036f)
20. Benabbou AK, Derriche Z, Felix C, Lejeune P, Guillard C. 2007 Photocatalytic inactivation of *Escherischia coli*. *Appl. Catal. B: Environ.* **76**, 257–263. (doi:10.1016/j.apcatb.2007.05.026)
21. Su C, Hong BY, Tseng CM. 2006 Sol–gel preparation and photocatalysis of titanium dioxide. *Catal. Today* **96**, 119–126. (doi:10.1016/j.cattod.2004.06.132)
22. Li Y-F, Liu Z-P. 2011 Particle size, shape and activity for photocatalysis on titania anatase nanoparticles in aqueous surroundings. *J. Am. Chem. Soc.* **133**, 15 743–15 752. (doi:10.1021/ja206153v)
23. Satoh N, Nakashima T, Kamikura K, Yamamoto K. 2008 Quantum size effect in TiO_2 nanoparticles prepared by finely controlled metal assembly on dendrimer templates. *Nat. Nanotechnol.* **3**, 106–111. (doi:10.1038/nnano.2008.2)
24. Nam HJ, Amemiya T, Murabayashi M, Itoh K. 2004 Photocatalytic activity of sol—gel TiO_2 thin films on various kinds of glass substrates: the effects of Na^+ and primary particle size. *J. Phys. Chem. B* **108**, 8254–8259. (doi:10.1021/jp037170t)
25. Zhang Q, Gao L. 2003 Preparation of oxide nanocrystals with tunable morphologies by the moderate hydrothermal method: insights from rutile TiO_2. *Langmuir* **19**, 967–971. (doi:10.1021/la020310q)
26. Serrano DP, Calleja G, Sanz R, Pizarro P. 2004 Preparation of bimodal micro-mesoporous TiO_2 with tailored crystalline properties. *Chem. Commun.* **8**, 1000–1001. (doi:10.1039/B315493A)
27. Zhang D, Qi L, Ma J, Cheng H. 2002 Formation of crystalline nanosized titania in reverse micelles at room temperature. *J. Mater. Chem.* **12**, 3677–3680. (doi:10.1039/b206996b)
28. Sofia J, Islam M, Mujahid M. 2019 Synthesis and characterization of TiO_2 quantum dots by sol gel reflux condensation method. *Ceram. Int.* **45**, 2676–2679. (doi:10.1016/j.ceramint.2018.10.163)
29. Xu X, Gao Z, Cui Z, Liang Y, Li Z, Zhu S, Ma J. 2016 Synthesis of Cu_2O octadecahedron/TiO_2 quantum dot heterojunctions with high visible light photocatalytic activity and high stability. *ACS Appl. Mater. Interfaces* **8**, 91–101. (doi:10.1021/acsami.5b06536)
30. Lalitha G, Hemamalini R, Ravichandran K. 2015 Synthesis and characterization of TiO_2 quantum dots for photocatalytic application. *J. Saudi Chem. Soc.* **19**, 589–594. (doi:10.1016/j.jscs.2015.05.002)
31. Deng Q, Zhang W, Lan T, Xie J, Xie W, Liu Z, Huang Y, Wei M. 2018 Anatase TiO_2 quantum dots with a narrow band gap of 2.85eV based on surface hydroxyl groups exhibiting significant

photodegradation property. *Eur. J. Inorg. Chem.* **2018**, 1506–1510. (doi:10.1002/ejic.201800097)

32. Ela SE, Cogal S, Icli S. 2009 Conventional and microwave-assisted synthesis of ZnO nanorods and effects of PEG400 as a surfactant on the morphology. *Inorg. Chim. Acta* **362**, 1855–1858. (doi:10.1016/j.ica.2008.08.038)
33. Murugan AV, Samuel V, Ravi V. 2006 Synthesis of nanocrystalline anatase TiO_2 by microwave hydrothermal method. *Mater. Lett.* **60**, 480. (doi:10.1016/j.matlet.2005.09.017)
34. Oskam G, Nellore A, Lee Penn R, Searson PC. 2003 The growth kinetics of TiO_2 nanoparticles from titanium(IV) alkoxide at high water/titanium ratio. *J. Phys. Chem. B* **107**, 1734–1738. (doi:10.1021/jp021237f)
35. Khan MM, Ansari SA, Pradhan D, Han DH, Lee J, Cho MH. 2014 Defect-induced band gap narrowed CeO_2 nanostructures for visible light activities. *Ind. Eng. Chem. Res.* **53**, 9754–9763. (doi:10.1021/ie500986n)
36. Bai YY, Lu Y, Liu JK. 2016 An efficient photocatalyst for degradation of various organic dyes: Ag@Ag_2MoO_4-AgBr composite. *J. Hazard. Mater.* **307**, 26–35. (doi:10.1016/j.jhazmat.2015.12.052)
37. Mogyorosi K, Dekany I, Fendler JH. 2003 Preparation and characterization of clay mineral intercalated titanium dioxide nanoparticles. *Langmuir* **19**, 2938–2946. (doi:10.1021/la025969a)
38. Periyat P, Baiju KV, Mukundan P, Pillai PK, Warrier KGK. 2008 High temperature stable mesoporous anatase TiO_2 photocatalyst achieved by silica addition. *Appl. Catal. A: Gen.* **349**, 13–19. (doi:10.1016/j.apcata.2008.07.022)
39. Mikami M, Arakanura S, Kitao O, Arakwa H. 2002 Lattice dynamics and dielectric properties of TiO_2 anatase: a first-principles study. *Phys. Rev. B* **66**, 155213. (doi:10.1103/PhysRevB.66.155213)
40. Bersani D, Lottici PP, Ding X-Z. 1998 Phonon confinement effects in the Raman scattering by TiO_2 nanocrystals. *Appl. Phys. Lett.* **72**, 73–75. (doi:10.1063/1.120648)
41. Zou L, Luo Y, Hooper M, Hu E. 2006 Removal of VOCs by photocatalysis process using adsorption enhanced TiO_2–SiO_2 catalyst. *Chem. Eng. Process.* **45**, 959–964. (doi:10.1016/j.cep.2006.01.014)
42. Yan L, Hoffmann M, Yelamanchili RS, Terrenoire A, Schrinner M, Drechsler M, Möller MW, Breu J, Ballauff M. 2009 Well-defined crystalline TiO_2 nanoparticles generated and immobilized on a colloidal nanoreactor. *Macromol. Chem. Phys.* **210**, 377–386. (doi:10.1002/macp.200800608)
43. Suttiponparnit K, Jiang J, Sahu M, Suvachittanont S, Charinpanitku T, Biswas P. 2011 Role of surface area, primary particle size, and crystal phase on titanium dioxide nanoparticle dispersion properties. *Nanoscale Res. Lett.* **6**, 27. (doi:10.1007/s11671-010-9772-1)
44. Lee BC *et al.* 2009 Aquatic toxicity evaluation of TiO_2 nanoparticle produced from sludge of $TiCl_4$ flocculation of wastewater and seawater. *J. Nanopart. Res.* **11**, 2087–2096. (doi:10.1007/s11051-008-9574-x)
45. Kim HJ, Shul YG, Han HS. 2005 photocatalytic properties of silica-supported TiO_2. *Top. Catal.* **35**, 287–293. (doi:10.1007/s11244-005-3836-y)
46. Sawai J, Himizu K, Yamamoto O. 2005 Kinetics of bacterial death by heated dolomite powder slurry. *Soil Biol. Biochem.* **37**, 1484–1489. (doi:10.1016/j.soilbio.2005.01.011)
47. Zhao J, Yang X. 2003 Photocatalytic oxidation for indoor air purification: a literature review. *Build. Environ.* **38**, 645–654. (doi:10.1016/S0360-1323(02)00212-3)
48. Sunada K, Watanabe T, Hashimoto K. 2003 Studies on photokilling of bacteria on TiO_2 thin film. *J. Photochem. Photobiol. A: Chem.* **156**, 227–233. (doi:10.1016/S1010-6030(02)00434-3)
49. Fujishima A, Rao TN, Tryk DA. 2000 Titanium dioxide photocatalysis. *J. Photochem. Photobiol. C: Photochem. Rev.* **1**, 1–21. (doi:10.1016/S1389-5567(00)00002-2)
50. Nguyen VNH, Amal R, Beydoun D. 2006 Photodeposition of CdSe using Se-TiO_2 suspensions as photocatalysts. *J. Photochem. Photobiol. A: Chem.* **179**, 57–65. (doi:10.1016/j.jphotochem.2005.07.012)
51. Fujishima A, Hashimoto K, Watanabe T. 1999 *TiO_2 photocatalysis: fundamentals and applications*, English edn. Tokyo, Japan: BKC.
52. Ahmed F, Awada C, Ansari SA, Aljaafari A, Alshoaibi A. 2019 Data from: Photocatalytic inactivation of *Escherischia coli* under UV light irradiation using large surface area anatase TiO_2 quantum dots. Dryad Digital Repository. (doi:10.5061/dryad.9pc7mj1)